Journal of Computational Science 90 (2025) 102654

Contents lists available at ScienceDirect

Journal of Computational Science

journal homepage: www.elsevier.com/locate/jocs

A pseudospectral method for time-fractional PDEs with shifted Chebyshev and Lagrange interpolating polynomials on overlapping decomposed domains

Nancy Mukwevho [a,c], Olumuyiwa Otegbeye [b,*], Shina Daniel Oloniiju [a]

[a] Department of Mathematics, Rhodes University, Makhanda, PO Box 94, Grahamstown 6140, South Africa
[b] School of Computer Science and Applied Mathematics, University of Witwatersrand, Johannesburg, South Africa
[c] Department of Mathematical and Computational Sciences, University of Venda, Private Bag X5050, Thohoyandou, 0950, South Africa

ARTICLE INFO

Keywords:
Pseudospectral method
Time fractional partial differential equations
Thermal diffusion

ABSTRACT

Time-fractional partial differential equations (TFPDEs) are powerful mathematical tools for modeling a wide range of physical and biological phenomena that exhibit memory effects, anomalous diffusion and non-local behavior. These classes of equations are crucial in capturing dynamics where the influence of past states affects future evolution, making them essential in many areas of applied science, such as heat transfer, viscoelasticity and anomalous diffusion. This study proposes a pseudospectral method that combines the weighted sums of the Chebyshev and Lagrange polynomials to numerically approximate the solutions of TFPDEs. The spatial domain is partitioned into uniform, overlapping subdomains, where the solution in each subdomain is represented as a weighted sum of the Lagrange interpolating polynomials. On the other hand, the time domain is treated as a whole without decomposition, and the solution in the temporal dimension is expanded using the first-kind shifted Chebyshev polynomials. We validate the accuracy and performance of the method through a series of test cases, covering both linear and nonlinear TFPDEs in one and multiple spatial dimensions. These examples showcase the method's capability to handle the computational challenges associated with TFPDEs and underline its potential for broader applications in problems involving fractional dynamics. Specifically, the proposed technique is applied to resolve TFPDE, which models heat transfer on a disk, a problem relevant to modeling heat conduction in circular plates and semiconductor wafers. A time-dependent Gaussian heat source concentrated in a specific region of the disk is introduced to accurately simulate practical thermal diffusion dynamics. The gradual increase of the source term over time offers a more realistic representation of the evolving thermal diffusion process.

1. Introduction

The calculus of arbitrary real orders, involving integrals and derivatives of fractional orders, finds extensive applications within many disciplines such as engineering, science, biology and optics [1]. A thorough review exploring several practical applications of fractional calculus across science and engineering was provided by Sun et al. [2]. The article provided summaries of applications of fractional calculus authored by renowned researchers. Tenreiro Machado et al. [3] explored how fractional calculus can be applied in areas such as controller tuning, legged and redundant robots, heat diffusion, and the synthesis of digital circuits. The study acknowledged the benefit of using mathematical tools in modeling and controlling dynamical systems, with results highlighting the significance of fractional calculus and inspiring the evolution of new applications. Srivastava et al. [4] introduced an analytical method for vibration equations involving fractional-order differential operators. The study applied the q-homotopy approach to examine a fractional model for large membranes. Furthermore, the Laplace-based decomposition technique was used to solve an arbitrary real-order vibration equation. The findings indicated that the suggested methods are effective for fractional-order problems, with the degree of the fractional-time derivative having a crucial impact on displacement. Jacobs and Harley [5] explored the use of nonlinear TFPDEs in image processing through hybridization of the Laplace transform and pseudospectral approach. The application of TFPDEs to image processing validated the use of arbitrary differential operators in real-world problems, emphasizing the role of fractional-order derivatives as an extra control parameter. These derivatives notably influenced both the model's transition time and the

* Corresponding author.
E-mail addresses: nancy.mukwevho@univen.ac.za (N. Mukwevho), olumuyiwa.otegbeye@wits.ac.za (O. Otegbeye), s.oloniiju@ru.ac.za (S.D. Oloniiju).

https://doi.org/10.1016/j.jocs.2025.102654
Received 27 February 2025; Received in revised form 19 May 2025; Accepted 13 June 2025
Available online 25 June 2025

final state achieved. Rashid et al. [6] proposed a numerical method for solving time-fractional multi-dimensional partial differential equations commonly arising in physics and engineering. Their approach, based on the fractional natural decomposition method (FNDM), was applied to a variety of time-dependent fractional-order models, including telegraph, parabolic, sine-Gordon, and wave-like equations. The method successfully produced solutions, showcasing its effectiveness in handling complex nonlinear systems. It was shown to be accurate, explicit, and suitable for modeling a wide range of practical problems. In several cases, closed-form and exact solutions were obtained. Furthermore, a comparative analysis emphasized the novel aspects introduced by incorporating hybrid fractional derivatives into the modeling framework. Fractional biological models were analyzed using time-fractional differential equations by Singh et al. [7] and Srivastava et al. [8], where Singh et al. [7] developed the Sumudu transform method and homotopy perturbation for solving nonlinear fractional PDEs that model spatial diffusion in biological populations. The model describes patterns of animal movement, and the resulting solutions were compared with those derived from the Sumudu decomposition method. The results showed that the proposed approach is both straightforward to implement and capable of producing accurate solutions. Srivastava et al. [8] proposed a time-fractional biological population model formulated using the Caputo fractional derivative. The model was solved using the fractional reduced differential transform method (FRDTM), through which both exact and approximate closed-form solutions were derived. The results demonstrated that FRDTM is not only straightforward to implement but also highly efficient in terms of computational cost.

Analytical techniques have been utilized to solve time-fractional differential equations. We refer readers to Kaplan and Bekir [9] and Alderremy et al. [10]. Bekela et al. [11] used the concept of Laplace-like transformation and variational theory to develop the Laplace transform variational iteration technique for nonlinear TFPDEs. The convergence and stability of the technique were examined within the framework of Banach spaces. The method performed much better than the HPM, HPTM, RPSM and HATM. Nawaz et al. [12] investigated approximate solutions of fractional order partial differential equations using a newly introduced semi-analytical approach known as the optimal auxiliary function method. The method was applied to the time-fractional Fisher equation, the time-fractional Fornberg–Whitham equation, and the time-fractional inviscid Burgers equation. A key advantage of the method was that it does not require discretization or the assumption of small or large parameters, and it yields approximate solutions after only a single iteration. The numerical results obtained were compared with those from HPTM.

Given the challenge of obtaining precise analytical solutions for most fractional differential equations, numerous numerical techniques to approximate their solutions have been proposed [13]. Lin et al. [14] proposed an iterative method based on modified radial basis functions (RBFs) for solving nonlinear time-fractional Benjamin–Bona–Mahony–Burgers equations on arbitrary domains. The approach integrates a quasi-linearization technique to address the nonlinearity and introduces a novel strategy for solving fractional ordinary differential equations. Spatial discretization is performed using a meshless backward substitution method, while the temporal domain is approximated using the Müntz polynomial basis. The method's effectiveness is demonstrated through a series of test problems involving up to three spatial dimensions, showing high accuracy, robustness, and computational efficiency. The results underscore the potential of RBF-based methods in handling complex, multidimensional time-fractional PDEs on irregular domains. Lin et al. [15] developed a meshless method for solving time-fractional partial differential equations (TFPDEs) with general spatial operators in both 2D and 3D regular and irregular domains. The method constructs the spatial approximation as a truncated series expansion using a set of linearly independent functions. The resulting system is then solved through a backward substitution technique based on modified basis functions. The primary goal was to demonstrate the method's accuracy and efficiency, which was supported by numerical results from various 2D and 3D test examples. Ahmad et al. [16] introduced a fractional iteration algorithm for non-linear TFPDEs. The method was developed and applied to the nonlinear fractional-order Fornberg–Whitham equation, without relying on transformations, Adomian polynomials, small perturbation techniques, discretization, or linearization. The fractional derivatives in the model were considered in the Caputo sense. To evaluate the effectiveness and accuracy of the proposed method, numerical results were compared with those obtained from the standard variational iteration method and with the exact solution. Furthermore, different values of the fractional-order parameter α demonstrated the robustness and applicability of the method. The findings indicated that the proposed scheme is highly effective, well-suited for solving fractional PDEs, and can be viewed as a generalization of existing methods for both integer- and noninteger-order differential equations. Herrera et al. [17] proposed a novel approach combining implicit finite difference discretization and a mimetic finite difference approximation to solve the time-fractional Caputo derivative, while Roul et al. [18] developed a numerical method using a uniform mesh to solve a diffusion equation with a time-fractional derivative. The transform-based decomposition method was used to solve TFPDEs by Saadeh et al. [19]. Comparison with other methods speaks to the efficiency and applicability of the formable transform decomposition method. Hayat et al. [20] used a hybrid approach combining the homotopy perturbation and Laplace transforms methods to solve systems of TFPDEs. The study demonstrated that the proposed method is both efficient and reliable for any class of TFPDEs, whether linear or nonlinear.

Spectral methods are a class of numerical techniques that express the solution of differential equations as a weighted sum of orthogonal polynomials. These polynomials, such as Chebyshev polynomials, are eigenvalue solutions of the Sturm–Liouville problem. One key advantage of spectral methods is the spectral rate of convergence for differential equations with sufficiently smooth solutions, where the error decreases exponentially as the number of modes or polynomials increases. This exponential rate of convergence makes this class of numerical techniques highly efficient for solving differential equations. Spectral methods are particularly well-suited for differential equations with arbitrary non-integer orders because spectral methods are inherently global approximations, which use global basis functions, and this makes them naturally aligned with the global nature of fractional differential operators, allowing for a more accurate approximation. The literature abounds with some studies that explore the applications of spectral-based techniques to TFPDEs, whether as hybridization with other analytical or numerical methods or as a standalone spectral method for direct solution approximation. Shokri and Mirzaei [21] presented the implementation of a pseudospectral method based on Lagrange polynomials for the numerical analysis of multi-term time-fractional differential equations. A semi-discrete approximation scheme was used to transform the original problem into a system of ordinary fractional differential equations. To preserve the high accuracy characteristic of spectral methods, the Mittag-Leffler function was used for time integration, and the numerical results demonstrated the accuracy and efficiency of the proposed scheme. A numerical scheme based on the Galerkin method was proposed by Bin Jebreen and Cattani [22], for solving time-fractional partial differential equations. Chebyshev cardinal functions (CCFs) were introduced, and the Caputo fractional derivative was expressed in terms of these basis functions using the relation between fractional integrals and derivatives. By applying the Galerkin method, the fractional differential equation was reduced to a system of linear algebraic equations. The solution to the system provided the approximate solution to the original problem. A convergence analysis was carried out to validate the method, and numerical simulations were presented to demonstrate its accuracy and effectiveness. In the study by Abdelghany et al. [23], a spectral method was used to

solve the time-fractional diffusion equation. The approach utilized Lucas polynomials (LPs) within a Petrov–Galerkin framework to construct the basis for the solution. The core idea of the proposed technique was to transform the governing boundary-value problem into a system of linear algebraic equations using the Petrov–Galerkin method. Various numerical procedures can be applied to solve the resulting system. The accuracy and effectiveness of the method were demonstrated. Atta et al. [24] presented a method for solving the time-fractional Newell-Whitehead-Segel equation (TFNWSE), which has applications across various scientific domains. The approach involved expanding the exact solution in both temporal and spatial variables using a linear combination of basis functions specifically constructed to satisfy the homogeneous boundary and initial conditions. The basis functions were formulated using fourth-kind Chebyshev polynomials (CP4K), enabling an analytical framework for the method. Through rigorous mathematical derivations, explicit expressions for all necessary derivatives, including those involving hypergeometric functions were obtained. The spectral collocation method was then applied to discretize the equation, reducing it to a solvable algebraic system. A comprehensive error analysis was conducted to assess the accuracy and reliability of the proposed scheme. Atta and Youssri [25] used a combination of orthogonal Gegenbauer polynomials as basis functions that satisfy homogeneous boundary conditions in the spatial variable and homogeneous initial conditions in the temporal variable. Expressions were derived for both the fractional derivative of the temporal basis functions and the second-order derivative of the spatial basis functions. The nonlinear Fisher equation was then discretized using the spectral collocation method, reducing it to a nonlinear system of algebraic equations. The resulting system was then solved using the Newton's method, with an initial guess close to zero. An error analysis was carried out to evaluate the performance of the proposed approach, and its applicability was demonstrated.

Chen et al. [26] applied a multidomain spectral method to TFPDEs. The method proposed in the study offers a balance between high-order accuracy and computational cost and utilizes two integration and differentiation rules derived from the recursive equations of the Jacobi polynomials combined with high-degree Gaussian quadrature. The analysis confirmed optimal stability properties, with the results demonstrating hp-convergence. Variable-order TFPDEs in higher dimensions were solved by Ahmed and Hashem [27] using a spectral tau method. Operational matrices for variable-order fractional derivatives, along with the tensor product of space–time vectors, were formulated using shifted Gegenbauer polynomials. The findings confirmed that the spectral tau method is effective for discretizing the variable-order TFPDE while exhibiting the spectral accuracy typical of spectral-based methods. Atta et al. [28] presented two numerical methods for addressing the fractional initial value problem (FIVP) and the time-fractional partial differential problem (FPDP), both exhibiting exponentially rapid error decay. The proposed schemes were derived using the spectral Galerkin method, which reduced each problem to an algebraic system involving unknown expansion coefficients. The approach utilized Chebyshev polynomials of the fifth kind. Approximate solutions to the FIVP and FPDP were constructed using newly defined basis functions known as regular shifted Chebyshev poly-fractionomials of the fifth kind. Convergence and error analysis were conducted in detail for both problems.

This study examines TFPDEs of the form

$$ {}_0^C D_t^{\gamma} u(\mathbf{x},) = \mathcal{H}[u(\mathbf{x},t)], \quad \gamma \in \mathbb{R}_+, \ \mathbf{x} \in \mathbb{R}^2, \ t \in [0,h], \tag{1} $$

where $\mathcal{H}$ represents a nonlinear classical differential operator of $u(\mathbf{x},t)$ and its partial derivatives, with ${}_0^C D_t^{\gamma} u(\mathbf{x},t)$ denoting the differential operator of arbitrary real order. The linearization technique introduced by Bellman and Kalaba [29] is used to transform the non-linear differential equation into a linear form. This work uses the fractional differential operator in the Caputo sense, defined as follows:

$$ {}_0^C D_t^{\gamma} u(\mathbf{x},t) = \frac{1}{\Gamma(\lceil\gamma\rceil-\gamma)} \int_0^t (t-\tau)^{\lceil\gamma\rceil-\gamma-1} \frac{\partial^{\lceil\gamma\rceil} u(\mathbf{x},\tau)}{\partial t^{\lceil\gamma\rceil}} d\tau, \quad \gamma \in \mathbb{R}_+. \tag{2} $$

The current study proposes a pseudospectral method for solving the TFPDE (1), applying a summation of weighted Lagrange interpolating polynomials and the first-kind Chebyshev polynomials to approximate the solution in the spatial and temporal dimensions, respectively. The spatial domain is divided into uniform overlapping subdomains to improve computational accuracy and efficiency. Within each spatial subdomain, the differential equation's solution is approximated using the Lagrange interpolating polynomials. The temporal domain is discretized without decomposition with the solution of the TFPDE represented using the first-kind Chebyshev polynomials. This study presents numerical examples of different types of TFPDEs to illustrate the practicality and efficiency of the proposed technique. In addition, the proposed method is applied to the time-fractional thermal diffusion equation on a disk, which is relevant to modeling heat conduction in circular plates and semiconductor wafers. A localized, time-dependent Gaussian heat source is introduced, gradually increasing over time to simulate realistic thermal diffusion dynamics.

The article is organized in the following manner: Section 2 outlines numerical discretization technique in both spatial and temporal dimensions. Section 3 presents numerical examples, which include linear, non-linear and system of TFPDEs and the discussion of the results. Section 4 investigates the application of the pseudospectral method to heat transfer on a disk. Lastly, Section 5 provides the conclusions.

2. Numerical discretization of the time-fractional PDE

This section detailed a description of the discretization of the TFPDEs using hybridization of the Lagrange interpolating polynomial in the spatial dimension and the shifted first-kind Chebyshev polynomial for the temporal dimension.

2.1. Domain decomposition and discretization in one spatial dimension

The spatial domain $x \in [a,b]$ is divided into q overlapping subintervals of equal length, Ω_l such that:

$$ \Omega_l = [x_{l-1}, \bar{x}_l], \quad x_{l-1} < x_l < \bar{x}_l, \quad x_0 = a, \quad \bar{x}_q = b, \quad l = 1,2,\ldots,q, \tag{3} $$

where the notation $x_l < \bar{x}_l$ describes the overlapping nature of the subintervals. Each subinterval Ω_l overlaps with the subsequent subinterval Ω_{l+1} in the sense that the first two grid points of Ω_{l+1} overlap with the last two grid points of Ω_l. This overlap ensures the continuity and smoothness of the solution across the entire domain. The grid points in $x \in [a,b]$ are formed by the union of the grid points from all subintervals. If G_l denotes the grid points within the subinterval Ω_l, then G represents the full set of grid points across $x \in [a,b]$ given by:

$$ G = \bigcup_{l=1}^{q} G_l, \tag{4} $$

where each G_l consists of the grid points within the subinterval, Ω_l, which accounts for the overlap between consecutive subintervals. As a result, the set G_l encompasses all the grid points across the entire domain, including those that overlap between adjacent subintervals. Specifically, the first subinterval, Ω_1, spans from $a = x_0^{(1)}$ to $x_N^{(1)}$, where $x_N^{(1)} = x_1^{(2)}$ is the second grid point of the next subinterval Ω_2. The subsequent subintervals, Ω_l for $2 \le l \le q$, share two grid points with their adjacent subintervals: $x_0^{(l)} = x_{N-1}^{(l-1)}$ and $x_1^{(l)} = x_N^{(l-1)}$, and the final subinterval, Ω_q, ends at $x_N^{(q)} = b$, the right boundary of the domain. The decomposition of the domain, highlighting the overlapping subintervals and shared grid points, is illustrated in Fig. 1.

The physical domain $[x_{l-1}, \bar{x}_l]$ within the subinterval Ω_l is mapped onto the computational domain $\hat{x} \in [-1,1]$. This mapping allows the application of the standard Chebyshev pseudospectral approximation using the following linear transformation:

$$ \hat{x}(x) = \left(\frac{2x}{\bar{x}_l - x_{l-1}} - \frac{\bar{x}_l + x_{l-1}}{\bar{x}_l - x_{l-1}} \right), \quad x \in [x_{l-1}, \bar{x}_l]. \tag{5} $$

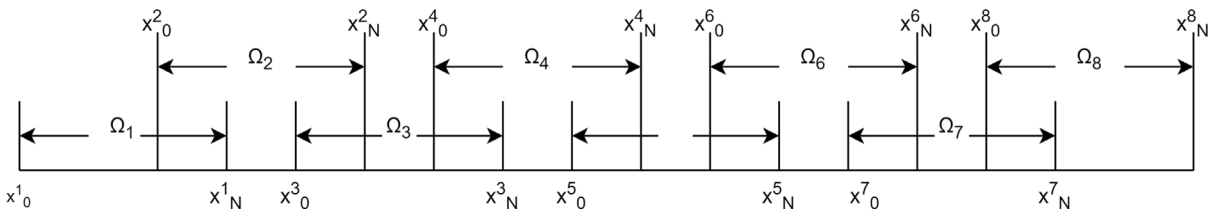

Fig. 1. Diagram of the spatial domain divided into eight equal subintervals with overlapping regions.

The subintervals are discretized into $(N+1)$ Chebyshev–Gauss–Lobatto (CGL) points. The discrete nodes within each subinterval for the $\hat{x}$ variable are given by:

$$\left\{\hat{x}_e\right\}_{e=0}^{N} = -\cos\left(\frac{e\pi}{N}\right). \tag{6}$$

Within the inner subintervals, the length of each subinterval, Ω_l, is expressed as $\mathfrak{L} = \bar{x}_l - x_{l-1}$ based on the total number of overlapping subintervals q. Since q overlapping subintervals result in $(q-1)$ overlapping regions, according to Eq. (4) each subinterval has length

$$\mathfrak{L} = \frac{b-a}{q + \frac{1-q}{2}\left(1 - \cos\left(\frac{\pi}{N}\right)\right)}. \tag{7}$$

Suppose $u(x)$ is continuously differentiable in the domain $[a,b]$. Specifically, the function $u(x)$ is interpolated using the Lagrange cardinal polynomials and evaluated at $N+1$ different CGL points, x_e, leading to the following approximation:

$$u(x) \approx U(x) = \sum_{n=0}^{N} U(x_n)\mathcal{L}_n(x_e), \tag{8}$$

with Lagrange cardinal polynomials $\mathcal{L}_n(x)$ defined as

$$\mathcal{L}_n(x) = \prod_{\substack{e=0 \\ e\neq n}}^{N} \frac{x - x_e}{x_n - x_e}, \quad \text{with} \quad \mathcal{L}_n(x_e) = \delta_{e,n} = \begin{cases} 1 & \text{if } n = e, \\ 0 & \text{if } n \neq e. \end{cases} \tag{9}$$

Differentiating Equation (8) with respect to x within each subinterval yields the spectral differentiation matrix, which serves as a discrete differential operator of the derivative of the function at the CGL points. The resulting derivative approximation is as follows:

$$\frac{du(x)}{dx} \approx \sum_{n=0}^{N} \overset{l}{d}_{e,n} U(x_n) = \overset{l}{\mathbf{d}}\mathbf{U},\ e = 0, 1, \ldots, N \tag{10}$$

where $\overset{l}{\mathbf{d}} = \frac{2}{\mathfrak{L}}\hat{\mathbf{d}}$, and $\hat{\mathbf{d}}$ is a matrix operator of size $(N+1)$-by-$(N+1)$ proposed by Trefethen [30] for approximating the first-order derivative of a function. The entries of this matrix are defined as follows:

$$\begin{cases} \hat{d}_{0,0} = -\hat{d}_{N,N} = \dfrac{2N^2+1}{6}, \\ \hat{d}_{e,n} = \dfrac{c_e(-1)^{n+e}}{c_n(x_e - x_n)}, \quad \text{for} \quad e \neq n,\ e, n = 0, \ldots, N, \\ \hat{d}_{n,n} = -\dfrac{x_n}{2(1-x_n^2)}, \quad \text{for} \quad n = 1, \ldots, N-1, \end{cases} \tag{11}$$

where $c_n = 2$, for $n = 0, N$ and $c_n = 1$, for $n = 1, \ldots, N-1$, with the vector $\mathbf{U} = [U(x_0^{(l)}), U(_1^{(l)}x), \ldots, U(x_N^{(l)})]^{\mathsf{T}}$ representing the discrete values of $u(x)$ at the points in the subdomain, Ω_l. Due to the overlap between subintervals Ω_l and Ω_{l+1}, the differentiation matrix $\mathbf{D}$ is constructed by eliminating specific rows associated with the shared nodes. This guarantees that the matrix only accounts for distinct grid points within the domain and avoids redundancy. As a result, the differentiation matrix is defined as (see the equation in Box I):

The matrix $\overset{l}{\mathbf{d}}$ is the differentiation matrix for the lth spatial subdomain, and all unfilled entries of $\mathbf{D}$ are explicitly set to zero. The overall matrix $\mathbf{D}$ has dimensions Q-by-Q, where $Q = (q-1)(N-1)+N$, with N representing the number of Chebyshev–Gauss–Lobatto points per subinterval and q represents the overall number of overlapping subintervals. In the multidomain framework, the grid points associated with the assembled differentiation matrix across the entire spatial domain are defined as follows:

$$\begin{aligned} &\{a = x_0^{(1)}, \ldots, x_{N-1}^{(1)}, x_1^{(2)}, \ldots, x_{N-1}^{(2)}, \ldots, x_1^{(l)}, \ldots, x_{N-1}^{(l)}, \ldots, \\ &\quad x_1^{(q)}, \ldots, x_N^{(q)} = b\}, \quad 3 \leq l \leq q-1. \end{aligned} \tag{12}$$

Higher-order derivatives are given through matrix powers as follows:

$$\frac{d^w u(x)}{dx^w} \approx \mathbf{D}^w\mathbf{U}. \tag{13}$$

2.2. Discretization in the temporal dimension

Suppose $u(t)$ is defined and continuously differentiable in the temporal domain $[0,h]$. The arbitrary function $u(t)$ is approximated using the first-kind Chebyshev polynomials, derived through the recurrence relation:

$$\begin{aligned} &\zeta_{h,0}(t) = 1, \quad \zeta_{h,1}(t) = \frac{2t}{h} - 1, \quad \zeta_{h,j+1}(t) = \left(\frac{4t}{h} - 2\right)\zeta_{h,j}(t) - \zeta_{h,j-1}(t), \\ &\quad j = 1, \ldots, . \end{aligned} \tag{14}$$

The function $u(t)$ is approximated over the domain $[0,h]$ using a truncated series expansion using the shifted Chebyshev polynomials, given by

$$u(t) \approx U_h(t) = \sum_{j=0}^{M} \hat{u}_j \zeta_{h,j}(t), \quad t \in [0,h], \tag{15}$$

in which $\zeta_{h,j}(t)$ represents the shifted Chebyshev polynomial defined in series form as

$$\zeta_{h,j}(t) = j\sum_{k=0}^{j}(-1)^{j-k}\frac{2^{2k}(j+k-1)!}{(2k)!(j-k)!h^k}t^k, \quad j > 0, \tag{16}$$

and the coefficients $\hat{u_j}$ in Eq. (15) are determined by a weighted sum as follows

$$\hat{u}_j = \langle U_h, \zeta_{h,j}\rangle = \frac{1}{\mu_j}\sum_{i=0}^{\infty} U_h(t_i)\zeta_{h,j}(t_i)\rho_i, \quad \text{with} \quad \mu_j = \begin{cases} \pi & j = 0 \\ \dfrac{\pi}{2} & j \neq 0. \end{cases} \tag{17}$$

By using a truncated Mth order approximation and $M+1$ distinct CGL points $0 \leq t_r \leq h$, where $r = 0, 1, \ldots, M$, $u(t)$ can then be approximated as:

$$
\mathbf{D} = \begin{bmatrix}
\overset{1}{d}_{0,0} & \overset{1}{d}_{0,1} & \cdots & \overset{1}{d}_{0,N-1} & \overset{1}{d}_{0,N} & & & & & \\
\vdots & \vdots & \vdots & \vdots & \vdots & & & & & \\
\overset{1}{d}_{N-1,0} & \overset{1}{d}_{N-1,1} & \cdots & \overset{1}{d}_{N-1,N-1} & \overset{1}{d}_{N-1,N} & & & & & \\
 & & & \overset{2}{d}_{1,0} & \overset{2}{d}_{1,1} & \cdots & \overset{2}{d}_{1,N-1} & \overset{2}{d}_{1,N} & & \\
 & & & \vdots & \vdots & \vdots & \vdots & \vdots & & \\
 & & & \overset{2}{d}_{N-1,0} & \overset{2}{d}_{N-1,1} & \cdots & \overset{2}{d}_{N-1,N-1} & \overset{2}{d}_{N-1,N} & & \\
 & & & & & & \ddots & \ddots & \ddots & \\
 & & & & & & & & \overset{q}{d}_{1,0} & \overset{q}{d}_{1,1} & \cdots & \overset{q}{d}_{1,N} \\
 & & & & & & & & \vdots & \vdots & \vdots & \vdots \\
 & & & & & & & & \overset{q}{d}_{N,0} & \overset{q}{d}_{N,1} & \cdots & \overset{q}{d}_{N,N}
\end{bmatrix}
$$

Box I.

$$
u(t) \approx \sum_{i=0}^{M} U_h(t_i)\rho_i \sum_{j=0}^{M} \frac{1}{\mu_j}\zeta_{h,j}(t_i)\zeta_{h,j}(t_r). \tag{18}
$$

The Christoffel coefficients ρ_i related to the Gauss–Lobatto (GL) quadrature, defined as

$$
\rho_i = \frac{\pi}{c_i M}, \quad \text{with} \quad c_i = \begin{cases} 2, & i = 0, M \\ 1, & 1 \le i \le M-1. \end{cases} \tag{19}
$$

From the following matrix representations

$$
\begin{cases}
\boldsymbol{P} = \begin{bmatrix} \rho_0 & & & \\ & \rho_1 & & \\ & & \ddots & \\ & & & \rho_M \end{bmatrix}, \quad \boldsymbol{T} = \begin{bmatrix} \frac{1}{\mu_0} & & & \\ & \frac{1}{\mu_1} & & \\ & & \ddots & \\ & & & \frac{1}{\mu_M} \end{bmatrix} \\
\boldsymbol{Z}_h = \begin{bmatrix} \zeta_{h,0}(t_0) & \zeta_{h,0}(t_1) & \cdots & \zeta_{h,0}(t_M) \\ \zeta_{h,1}(t_0) & \zeta_{h,1}(t_1) & \cdots & \zeta_{h,1}(t_M) \\ \vdots & \vdots & \ddots & \vdots \\ \zeta_{h,M}(t_0) & \zeta_{h,M}(t_1) & \cdots & \zeta_{h,M}(t_M) \end{bmatrix},
\end{cases} \tag{20}
$$

Eq. (18) can then be represented as

$$
u(t) \approxeq \sum_{i=0}^{M} U_h(t_i)E_i(t_r) = \mathbf{E}^{\top}\mathbf{U}_h, \tag{21}
$$

where $\mathbf{E} = \boldsymbol{P}\boldsymbol{Z}_h^{\top}\boldsymbol{T}\boldsymbol{Z}_h$ and the column vector $\mathbf{U}_h$ is the approximated values of $u(t)$ evaluated at the transformed CGL time points, $t_0, \ldots, t_M$. Subsequently, the approximation of the arbitrary real order derivative of $u(t)$ is formulated as follows:

$$
{}_0^C D_t^{\gamma} u(t) {}_0^C D_t^{\gamma} \approx U_h(t) \sum_{i=0}^{M} U_h(t_i)\rho_i \sum_{j=0}^{M} \frac{1}{\mu_j}\zeta_{h,j}(t_i) {}_0^C D_t^{\gamma}\zeta_{h,j}(t). \tag{22}
$$

The arbitrary non-integer derivative of the Chebyshev function, ${}_0^C D_t^{\gamma}$ $\zeta_{h,j},(t)$ is evaluated utilizing Eq. (16), so that:

$$
{}_0^C D_t^{\gamma}\zeta_{h,j}(t) = j \sum_{k=\lceil\gamma\rceil}^{j} \frac{\Gamma(k+1)}{\Gamma(k-\gamma+1)}(-1)^{j-k}\frac{2^{2k}(j+k-1)!}{(2k)!(j-k)!h^k}t^{k-\gamma}. \tag{23}
$$

Eq. (23) can be written as follows when $t^{k-\gamma}$ is expressed in terms of the shifted Chebyshev polynomials of first-kind:

$$
{}_0^C D_t^{\gamma}\ \zeta_{h,j}(t) = {}_h D^{\gamma}\boldsymbol{Z}_h \tag{24}
$$

where ${}_h D^{\gamma} = \boldsymbol{\Pi}\,\boldsymbol{\Lambda}\,\boldsymbol{\Psi}\,\boldsymbol{\Pi}^{\top}\boldsymbol{T}$ and the entries of the matrices $\boldsymbol{\Pi}$, $\boldsymbol{\Lambda}$ and $\boldsymbol{\Psi}$, are defined, respectively, as

$$
\left.
\begin{aligned}
\boldsymbol{\Pi}_{j,k} &= \begin{cases} 1 & \text{if } j = 0, k = 0 \\ (-1)^{j-k}\dfrac{j2^{2j}(j+k-1)!}{(2k)!(j-k)!h^k} & \text{if } j = 1, \ldots, M,\ k = 0, \ldots, j \\ 0 & \text{otherwise,} \end{cases} \\
\lambda_{k,k} &= \begin{cases} 0 & \text{if } \lceil\gamma\rceil > k \\ \dfrac{\Gamma(k+1)}{\Gamma(k-\gamma+1)} & \text{if } k = \lceil\gamma\rceil, \ldots, M, \end{cases} \\
\boldsymbol{\Psi}_{m,k} &= \begin{cases} 0 & \text{if } \lceil\gamma\rceil > k \\ \dfrac{\sqrt{\pi}h^{k-\gamma+m}\Gamma(k-\gamma+m+\frac{1}{2})}{\Gamma(k-\gamma+m+1)} & \text{if } k = \lceil\gamma\rceil, \ldots, M, \\ & m = 0, \ldots, p,\ p = 0, \ldots, M. \end{cases}
\end{aligned}
\right\} \tag{25}
$$

Therefore, the fractional derivative of $u(t)$, ${}_0^C D_t^{\gamma} u(t)$, is then approximated as

$$
{}_0^C D_t^{\gamma} u(t) \approx ({}_h\mathbf{D}^{\gamma})^{\top}\mathbf{U}_h, \tag{26}
$$

where ${}_h\mathbf{D}^{\gamma} = \boldsymbol{P}\,\boldsymbol{Z}_h^{\top}\boldsymbol{T}\,{}_h D^{\gamma}\,\boldsymbol{Z}_h$, and $({}_h\mathbf{D}^{\gamma})^{\top}$ is the matrix of fractional derivatives expressed using the first-kind Chebyshev polynomials defined for the temporal domain, $[0, h]$.[1]

2.3. Pseudospectral discretization of TFPDEs

This section details the discretization of (1 + 1) and (1 + 2) dimensional TFPDEs. First, we illustrate the linearization of the nonlinear TFPDE by applying the quasilinearization method developed by Bellman and Kalaba [29]. This linearization technique relies on the Newton–Raphson approach for solving algebraic systems, which expands the nonlinear component of the differential equation in a truncated linear

[1] When $\gamma \longrightarrow 1^{-}$, the fractional derivative converges to the classical first derivative. Since Chebyshev expansions are known to provide accurate and stable approximations for classical derivatives, the stability of the method is maintained as the method behaves like a standard method for solving ordinary differential equations (ODEs). When $\gamma \longrightarrow 0^{+}$, the fractional derivative gives less weight to past values. In this case, the method stays stable because the Chebyshev expansion still works well to capture the solution's behavior. The problem becomes similar to one with a low-order time derivative, so the solution changes slowly and remains stable.

Taylor series about an initial estimate of the solution. Consider the nonlinear TFPDE

$$ {}_0^C D_t^\gamma u = \mathcal{H}\left[u, u_x, u_y, u_{xx}, u_{yy}, \ldots\right] + g, \qquad 0 < \gamma \le 1, \quad 0 < t \le h, \quad (x, y) \in (a, b)^2, \tag{27} $$

where $\mathcal{H}$ represent a nonlinear operator and g is the source term. The quasilinearization technique operates under the assumption that the differences between the solutions of the differential equation and their partial derivatives at two consecutive iterative levels, s and $s+1$, denoted by $\{(u^{s+1}-u^s), (u_x^{s+1}-u_x^s), (u_y^{s+1}-u_y^s), (u_{xx}^{s+1}-u_{xx}^s), (u_{yy}^{s+1}-u_{yy}^s), \ldots\}$, is negligible for higher powers in the Taylor series expansion. Therefore, applying the quasilinearization technique to Eq. (27) results in the following iterative scheme

$$ {}_0^C D_t^\gamma u^{s+1} - \alpha^{0,s}u^{s+1} - \alpha^{1,s}u_x^{s+1} - \beta^{1,s}u_y^{s+1} - \alpha^{2,s}u_{xx}^{s+1} - \beta^{2,s}u_{yy}^{s+1} - \cdots = B^s, \tag{28} $$

where

$$ \left.\begin{aligned} &\alpha^{0,s} = \frac{\partial \mathcal{H}[\ldots]}{\partial u}, \ \alpha^{1,s} = \frac{\partial \mathcal{H}[\ldots]}{\partial u_x}, \ \beta^{1,s} = \frac{\partial \mathcal{H}[\ldots]}{\partial u_y}, \ \alpha^{2,s} = \frac{\partial \mathcal{H}[\ldots]}{\partial u_{xx}}, \\ &\beta^{2,s} = \frac{\partial \mathcal{H}[\ldots]}{\partial u_{yy}}, \\ &B^s = \mathcal{H}[\ldots] - \alpha^{0,s}u^s - \alpha^{1,s}u_x^s - \beta^{1,s}u_y^s - \alpha^{2,s}u_{xx}^s - \beta^{2,s}u_{yy}^s - \cdots + g, \end{aligned}\right\} \tag{29} $$

and $\mathcal{H}[\ldots]$ denotes the evaluation of the nonlinear operator at $(u^s, u_x^s, u_y^s, u_x^s, u_{yy}^s, \ldots)$. Eq. (28) can subsequently be discretized according to the approximation techniques outlined in Sections 2.1 and 2.2. The method converges if the initial guess is close enough to the exact solution and if the nonlinear problem satisfies conditions, like having a smooth solution.

2.3.1. Discretization of the (1 + 1)–dimensional TFPDE

This section focuses on the one-dimensional formulation of the TFPDE (27)

$$ {}_0^C D_t^\gamma u = \mathcal{H}\left[u, u_x, u_x, \ldots\right] + g, \qquad t \in (0, h], \quad x \in (a, b), \quad \gamma \in (0, 1), \tag{30} $$

with associated conditions. The solution to the TFPDE is represented as weighted sum of Lagrange and Chebyshev polynomials in the spatial and temporal dimensions, respectively, such that:

$$ u(x, t) = \sum_{i=0}^{M} \mathbf{E}_{r,i}\mathbf{U}_{h,i}, \tag{31} $$

where $\mathbf{U}_{h,i} = [\mathbf{U}_h(x_0, t_i), \ldots, \mathbf{U}_h(x_Q, t_i)]^\mathsf{T}$ and the entries of $\mathbf{E}_{r,i}$ are defined by the matrix $\mathbf{E}$ in Eq. (21). The spatial derivatives of $u(x, t)$ over the entire spatial domain is defined by Eq. (13) as

$$ \frac{\partial u}{\partial x} = \sum_{i=0}^{M} \mathbf{E}_{r,i}\mathbf{D}\mathbf{U}_{h,i} \quad \text{and} \quad \frac{\partial^2 u}{\partial x^2} = \sum_{i=0}^{M} \mathbf{E}_{r,i}\mathbf{D}^2\mathbf{U}_{h,i}. \tag{32} $$

The temporal fractional derivative of u is discretized at the collocation points using the $(M+1)$-by-$(M+1)$ differentiation matrix, as defined in Eq. (26)

$$ {}_0^C D_t^\gamma u = \sum_{i=0}^{M} ({}_h\mathbf{D}^\gamma)_{r,i}\,\mathbf{U}_{h,i}. \tag{33} $$

Therefore, the quasilinearized system of the algebraic equation that approximates the solution of Eq. (30) is given as

$$ \sum_{i=0}^{M}\left[({}_h\mathbf{D}^\gamma)_{r,i}\mathbf{I} - \boldsymbol{\alpha}^{0,s}\mathbf{E}_{r,i}\mathbf{I} - \boldsymbol{\alpha}^{1,s}\mathbf{E}_{r,i}\mathbf{D} - \boldsymbol{\alpha}^{2,s}\mathbf{E}_{r,i}\mathbf{D}^2 - \cdots\right]\mathbf{U}_{h,i}^{s+1} = \mathbf{B}_i^s, \quad r = 0(1)M, \tag{34} $$

where the identity matrix $\mathbf{I}$ is of the same as the spatial differentiation matrix, $\mathbf{D}$, $\mathbf{U}_{h,i}$ is the vector of discrete values, $[\mathbf{U}_{h,i}(x_0), \ldots, \mathbf{U}_{h,i}(x_Q)]^\mathsf{T}$, of $u(x, t)$ at different temporal points $\{t_i : i = 0, \ldots, M\}$, and the vectors, $\boldsymbol{\alpha}^{0,s}, \boldsymbol{\alpha}^{1,s}$ and $\boldsymbol{\alpha}^{2,s}$ are converted into diagonal matrices, $\boldsymbol{\alpha}^{0,s}, \boldsymbol{\alpha}^{1,s}$ and $\boldsymbol{\alpha}^{2,s}$, respectively, and $\mathbf{B}_i^s$ is the vector of discrete values defined by, $B^s = \mathcal{H}[\ldots] - \alpha^{0,s}u^s - \alpha^{1,s}u_x^s - \alpha^{2,s}u_{xx}^s - \cdots + f$, computed at the temporal discretization points, t_i. This algebraic system of equations is solved subject to the given prescribed conditions.

2.3.2. Discretization of the (1 + 2)–dimensional TFPDE

This section focuses on the two-dimensional formulation of the TFPDE (27). The quasilinearization technique is applied to linearize the nonlinear component, transforming the nonlinear differential equations into a series of linear equations. The method proposed in this study is then used to numerically solve the differential equation. This approach assumes that $u(x, y, t)$ can be written as a linear combination of basis functions. Specifically, in the spatial dimensions, the solution is expressed as a sum of Lagrange interpolating polynomials, which are well-suited for handling boundary conditions and capturing local variations in the spatial domain. In the temporal dimension, the solution is expanded using the first-kind shifted Chebyshev polynomials. The most straightforward approach to discretizing a two-spatial-dimensional differential equation using the spectral collocation method is to use the tensor product, which represents the spatial derivatives as a Kronecker product of the differentiation matrices associated with each dimension. Although this is efficient for matrix assembly and simplifies the formulation, the resulting system matrices are dense. Consequently, the memory usage grows approximately with $\mathcal{O}(N_x^2 N_y^2)$. Specifically, let $\mathbf{D}_x$ and $\mathbf{D}_y$ be the differentiation matrices on the overlapping grid corresponding to the derivatives in the x and y dimensions, respectively. The partial derivatives of u can then be written as:

$$ \begin{aligned} &\frac{\partial u}{\partial x} \approx \sum_{i=0}^{M} \mathbf{E}_{r,i}(\mathbf{D}_x \otimes \mathbf{I}_y)\mathbf{U}_{h,i}, \quad \frac{\partial u}{\partial y} \approx \sum_{i=0}^{M} \mathbf{E}_{r,i}(\mathbf{I}_x \otimes \mathbf{D}_y)\mathbf{U}_{h,i}, \\ &\frac{\partial^2 u}{\partial x^2} \approx \sum_{i=0}^{M} \mathbf{E}_{r,i}(\mathbf{D}_x^2 \otimes \mathbf{I}_y)\mathbf{U}_{h,i}, \quad \frac{\partial^2 u}{\partial y^2} \approx \sum_{i=0}^{M} \mathbf{E}_{r,i}(\mathbf{I}_x \otimes \mathbf{D}_y^2)\mathbf{U}_{h,i}, \end{aligned} \tag{35} $$

where $\otimes$ denotes the Kronecker product, $\mathbf{I}_x$ and $\mathbf{I}_y$ are identity matrices corresponding to the number of discrete points in the x and y domains, and $\mathbf{U}$ is the vectorized form of the solution on the two-dimensional grid. Upon applying the approximation techniques described in Sections 2.1 and 2.2, the discrete form of the (1 + 2)-dimensional time-fractional PDE is given as

$$ \left.\begin{aligned} \sum_{i=0}^{M}\Big[&({}_h\mathbf{D}^\gamma)_{r,i}(\mathbf{I}_x \otimes \mathbf{I}_y) - \boldsymbol{\alpha}^{0,s}\mathbf{E}_{r,i}(\mathbf{I}_x \otimes \mathbf{I}_y) - \boldsymbol{\alpha}^{1,s}\mathbf{E}_{r,i}(\mathbf{D}_x \otimes \mathbf{I}_y) \\ &- \boldsymbol{\beta}^{1,s}\mathbf{E}_{r,i}(\mathbf{I}_x \otimes \mathbf{D}_y) \\ &- \boldsymbol{\alpha}^{2,s}\mathbf{E}_{r,i}(\mathbf{D}_x^2 \otimes \mathbf{I}_y) - \boldsymbol{\beta}^{2,s}\mathbf{E}_{r,i}(\mathbf{I}_x \otimes \mathbf{D}_y^2) - \cdots\Big] \\ &\times \mathbf{U}_{h,i}^{s+1} = \mathbf{B}_i^s, \quad r = 0(1)M, \end{aligned}\right\} \tag{36} $$

where the vectorized forms of $\alpha^{0,s}, \alpha^{1,s}, \beta^{1,s}, \alpha^{2,s}, \beta^{2,s}$, defined on the spatial grid points, are converted into diagonal matrices, $\boldsymbol{\alpha}^{0,s}, \boldsymbol{\alpha}^{1,s}, \boldsymbol{\beta}^{1,s}$, $\boldsymbol{\alpha}^{2,s}, \boldsymbol{\beta}^{2,s}$, respectively, $\mathbf{B}^s$ is the vector of discrete values defined by the vectorized form of B^s defined in Eq. (29), which is then evaluated at each temporal collocation point, t_i and $\mathbf{U}_{h,i}$ is the vectorized form of the matrix of discrete values defined as

$$ \begin{bmatrix} \mathbf{U}_{h,i}(x_0, y_0) & \mathbf{U}_{h,i}(x_0, y_1) & \cdots & \mathbf{U}_{h,i}(x_0, y_Q) \\ \mathbf{U}_{h,i}(x_1, y_0) & \mathbf{U}_{h,i}(x_1, y_1) & \cdots & \mathbf{U}_{h,i}(x_1, y_Q) \\ \vdots & \vdots & \cdots & \vdots \\ \vdots & \vdots & \cdots & \vdots \\ \mathbf{U}_{h,i}(x_Q, y_0) & \mathbf{U}_{h,i}(x_Q, y_1) & \cdots & \mathbf{U}_{h,i}(x_Q, y_Q) \end{bmatrix}. \tag{37} $$

As in the one-dimensional case, Eq. (36) is solved subject to the discrete representation of the given conditions related to the TFPDE. This involves discretizing these conditions using the assumed form of the approximate solution.

Table 1
ℓ_∞ norm of the absolute difference error for Example 3.1 for varying values of γ, q, M, N and h.

γ	$M=15,\ N=30,\ h=1$				$N=30,\ h=3,\ q=6$				$M=15,\ h=2,\ q=6$			
	$q=3$	$q=5$	$q=7$	$q=9$	$M=5$	$M=10$	$M=15$	$M=18$	$N=15$	$N=20$	$N=30$	$N=50$
0.1	1.58×10^{-7}	1.55×10^{-7}	1.62×10^{-7}	1.68×10^{-7}	1.35×10^{-4}	1.39×10^{-5}	2.76×10^{-6}	1.41×10^{-4}	7.23×10^{-7}	7.25×10^{-7}	7.30×10^{-7}	8.47×10^{-7}
0.3	6.45×10^{-7}	6.52×10^{-7}	6.40×10^{-7}	6.45×10^{-7}	4.76×10^{-4}	6.27×10^{-5}	5.57×10^{-6}	6.76×10^{-5}	2.28×10^{-6}	2.28×10^{-6}	2.31×10^{-6}	2.63×10^{-6}
0.5	3.47×10^{-6}	3.47×10^{-6}	3.48×10^{-6}	3.50×10^{-6}	8.04×10^{-4}	1.30×10^{-4}	1.95×10^{-5}	2.80×10^{-5}	1.19×10^{-5}	1.19×10^{-5}	1.20×10^{-5}	1.20×10^{-5}
0.7	3.69×10^{-6}	3.70×10^{-6}	3.70×10^{-6}	3.72×10^{-6}	8.96×10^{-4}	1.97×10^{-4}	2.30×10^{-5}	1.57×10^{-4}	1.14×10^{-5}	1.14×10^{-5}	1.14×10^{-5}	1.15×10^{-5}
0.9	2.36×10^{-6}	2.36×10^{-6}	2.36×10^{-6}	2.35×10^{-6}	4.96×10^{-4}	1.54×10^{-4}	1.72×10^{-5}	7.01×10^{-4}	7.37×10^{-6}	7.42×10^{-6}	7.44×10^{-6}	7.40×10^{-6}

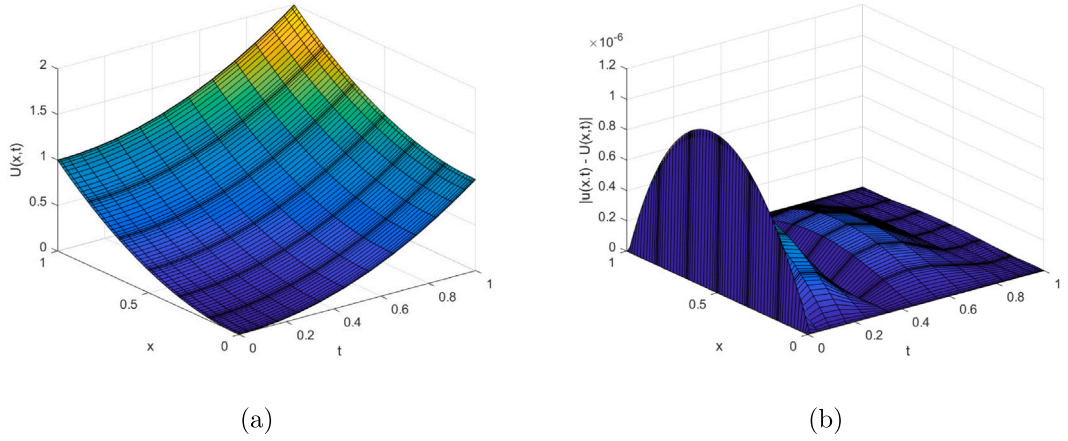

Fig. 2. The approximate solution and $|u-U|$ for Example 3.1 with $\gamma=0.5$, $M=N=15$, $q=6$ and $h=1$.

3. Illustrative examples and discussion

This section provides numerical examples to demonstrate the application of the proposed discretization techniques for various TFPDEs. The examples encompass a range of TFPDEs, including linear, nonlinear, and systems of equations, covering both one-dimensional and two-dimensional cases. The results are provided in tabular and graphical forms for a comprehensive analysis. To evaluate the accuracy of the numerical solution, we calculate the ℓ_∞ norm of the residual error, as well as the ℓ_∞ norm and ℓ_2 norm of the absolute difference error. The residual error, $R_{e,r}$, at each grid point, (x_e,t_r), for the (1+1)-dimensional case, is defined as

$$R_{e,r} = Res[U(x_e,t_r)] = \mathbf{AU}-\mathbf{B}, \tag{38}$$

and the ℓ_∞ norm of the residual error is defined as

$$\|R\|_\infty = \max_{e,r}|R_{e,r}|. \tag{39}$$

In general, for the (1+2)-dimensional case, the residual error, $R_{e,g,r}$, at each grid point (x_e,y_g,t_r), is defined as

$$R_{e,g,r} = Res[U(x_e,y_g,t_r)] = \mathbf{AU}-\mathbf{B}, \tag{40}$$

and the ℓ_∞ norm of the residual error is defined as

$$\|R\|_\infty = \max_{e,g,r}|R_{e,g,r}|. \tag{41}$$

If the exact solution at each grid x_e,y_g,t_r is defined as $u(x_e,y_g,t_r)$ and the approximate solution is defined as $U(x_e,y_g,t_r)$, then the absolute difference error, $\varepsilon_{e,g,r}$ at each grid point is defined as

$$\varepsilon_{e,g,r} = u(x_e,y_g,t_r) - U(x_e,y_g,t_r), \tag{42}$$

and the ℓ_∞ and ℓ_2 norms are, respectively, defined as

$$\|\varepsilon\|_\infty = \max_{e,g,r}|\varepsilon_{e,g,r}| \quad \text{and} \quad \|\varepsilon\|_2 = \left(\sum_{e,g,r}|\varepsilon_{e,g,r}|^2\right)^{1/2}. \tag{43}$$

We now proceed with approximating the solutions of TFPDEs using the proposed technique.

Example 3.1. We consider the linear TFPDE presented by Bin Jebreen and Cattani [22]

$${}_0^C D_t^\gamma u + \frac{\partial u}{\partial x} - \frac{\partial^2 u}{\partial x^2} = g(x,t), \quad t\ge 0,\ 0\le x\le 1,\ 0<\gamma\le 1,$$

subject to $u(0,t)=t^2$, $u(1,t)=t^2+1$, $t\ge 0$ and $u(x,0)=x^2$, $0\le x\le 1$, whose analytical solution is given as $u(x,t)=x^2+t^2$. In the above equation, $g(x)=2\frac{t^{2-\gamma}}{\Gamma(3-\gamma)}+2x-2$.

Table 1 depicts the infinity norm of the absolute difference error for varied values of q, M, N and h for Example 3.1. The reliability of the numerical approach is evaluated through the ℓ_∞ norm of the absolute difference error for varying γ values. Table 1 demonstrates that the results are accurate for the selected number of subintervals, q, in the spatial domain. The accuracy of the proposed method improves as h and M increase, confirming the need for higher temporal resolution over longer time intervals. Additionally, as N increases, the ℓ_∞ norm of the absolute difference error decreases. This demonstrates the reliability of the approach in solving the TFPDE, with its effectiveness particularly evident in the overlapping subdomains. Fig. 2 illustrates the characteristics of the approximate solutions and the absolute value of the difference between the exact and approximate solutions for Example 3.1. The figure shows that the approximate solutions closely match the exact solutions, confirming the accuracy and reliability of the proposed approach in solving the TFPDE.

Example 3.2. This example considers the linear TFPDE presented in [22]

$${}_0^C D_t^\gamma u + \frac{\partial u}{\partial x} = g(x,t), \quad t>0,\ -2\pi\le x\le 2\pi,\ 0<\gamma\le 1,$$

governed by the following conditions $u(-2\pi,t)=u(2\pi,t)=0$ and $u(x,0)=0$, and whose analytic solution is explicitly expressed as $u=t\sin x$, and $g(x,t)=\frac{t^{1-\gamma}}{\Gamma(2-\gamma)}\sin x+t\cos x$

Table 2 presents the infinity norm of the absolute difference error for Example 3.2 for distinct values of γ, q, M and N. With an increase in q and a decrease in γ, the numerical scheme confirms its accuracy. Furthermore, it is noticed that as M increases, the numerical technique

Table 2
Maximum value of the absolute difference error for Example 3.2 for various values of γ, q, M, N and h.

γ	$M = 15,\ N = 30,\ h = 1$				$N = 30,\ h = 1,\ q = 6$			$M = 15,\ h = 1,\ q = 6$			
	$q = 4$	$q = 6$	$q = 8$	$q = 10$	$M = 14$	$M = 16$	$M = 18$	$N = 15$	$N = 25$	$N = 35$	$N = 45$
0.1	7.67×10^{-5}	7.67×10^{-5}	7.62×10^{-5}	7.69×10^{-5}	8.67×10^{-5}	6.04×10^{-5}	1.17×10^{-4}	7.34×10^{-5}	7.61×10^{-5}	7.73×10^{-5}	7.79×10^{-5}
0.2	1.65×10^{-4}	1.65×10^{-4}	1.65×10^{-4}	1.66×10^{-4}	2.96×10^{-4}	3.20×10^{-4}	9.92×10^{-5}	1.58×10^{-4}	1.64×10^{-4}	1.66×10^{-4}	1.67×10^{-4}
0.3	2.22×10^{-4}	2.22×10^{-4}	2.22×10^{-4}	2.22×10^{-4}	3.58×10^{-4}	1.59×10^{-4}	2.42×10^{-4}	2.12×10^{-4}	2.20×10^{-4}	2.23×10^{-4}	2.24×10^{-4}
0.4	3.96×10^{-4}	3.97×10^{-4}	3.98×10^{-4}	3.99×10^{-4}	4.83×10^{-4}	3.01×10^{-4}	2.99×10^{-4}	3.87×10^{-4}	3.95×10^{-4}	4.00×10^{-4}	4.02×10^{-4}

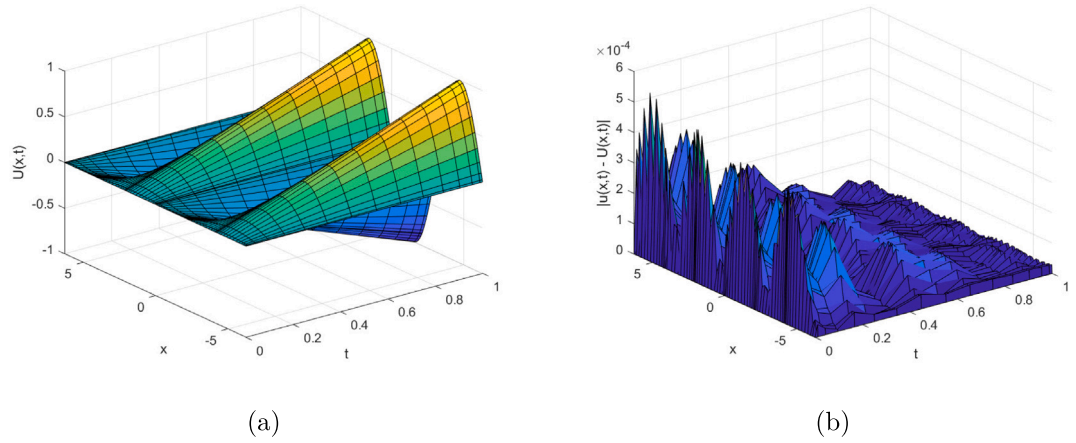

Fig. 3. The approximate solution and $|u - U|$ for Example 3.2 with $\gamma = 0.5$, $M = N = 15$, $q = 6$ and $h = 1$.

remains accurate. With different values of γ, the numerical technique remains accurate as N increases. The approximate solution and the absolute difference error for Example 3.2 are visually shown in Fig. 3 for the same values of M and N.

Example 3.3. Let us now consider the non-linear TFPDE in [31]

$$ {}_0^C D_t^\gamma u = \frac{\partial^2 u}{\partial x^2} + 6u(1-u), \quad 0 \le x \le 1, \quad 0 < \gamma \le 1, \quad t > 0, $$

subject to $u(0,t) = \frac{1}{(1+e^{-5t})^2}$, $u(1,t) = \frac{1}{(1+e^{1-5t})^2}$ and $u(x,0) = \frac{1}{(1+e^{x})^2}$ and whose explicit solution at $\gamma = 1$ is given as $u(x,t) = \frac{1}{(1+e^{x-5t})^2}$. The differential equation is linearized through the linearization technique described in Section 2.3.

Table 3 shows the ℓ_2 and ℓ_∞ norm of the residual error for Example 3.3, with $M = 10$, $N = 20$, $h = 1$, $q = 3$, with different values of γ. The ℓ_2 and ℓ_∞ norms are small. This trend indicates that the method maintains stability and accuracy when applied to fractional cases, not just the integer case ($\gamma = 1.0$). The results indicate that the method performs efficiently across different values of γ, with low error and reasonable computation times, all under 0.25 s. Table 4 presents the numerical solutions for distinct values of γ at various time (t) and spatial (x) points, with $M = 10$, $N = 20$, $h = 1$, $q = 3$. Additionally, the table includes the numerical and exact solutions for $\gamma = 1.0$. The findings indicate that the numerical approach is capable of producing exceptionally precise solutions, particularly for $\gamma = 1.0$, with the numerical solution matching the exact solution. As γ decreases, the solution starts to deviate, suggesting that γ has a noticeable impact on the solution, particularly for large values of t and x. The results at $x = 0$ and $x = 1$ are consistent across all the values of γ, indicating the reliability of the method at the boundaries.

Example 3.4. The homogeneous system of linear time-fractional PDEs is considered in this example [32]

$$ {}_0^C D_t^\gamma u - v_x + (u+v) = 0, \qquad {}_0^C D_t^\gamma v - u_x + (u+v) = 0, $$

governed by the following conditions: $u(x,0) = \sinh(x)$, $v(x,0) = \cosh(x)$, $u(0,t) = \sinh(-t)$, $u(1,t) = \sinh(1-t)$, $v(0,t) = \cosh(-t)$ and $v(1,t) = \cosh(1-t)$. At $\gamma = 1$, the analytic solutions are $u(x,t) = \sinh(x-t)$ and $v(x,t) = \cosh(x-t)$.

Table 3
ℓ_2 and ℓ_∞ norms of the residual errors for Example 3.3 for $M = 10$, $N = 20$, $q = 3$, $h = 1$, with various values of γ.

	$\gamma = 0.1$	$\gamma = 0.5$	$\gamma = 0.7$	$\gamma = 1.0$
ℓ_2 norm	1.17×10^{-10}	2.05×10^{-10}	1.56×10^{-10}	1.66×10^{-10}
ℓ_∞ norm	3.28×10^{-10}	1.12×10^{-9}	7.87×10^{-10}	5.21×10^{-10}
CPU time (s)	0.189	0.224	0.239	0.186

Table 4
Numerical solutions of Example 3.3 for $M = 10$, $N = 20$, $q = 3$, and $h = 1$ with varying values of γ, t, and x.

t	x	$\gamma = 0.1$	$\gamma = 0.5$	$\gamma = 0.7$	$\gamma = 1.0$	Exact ($\gamma = 1.0$)
0.5	0.0	0.8540	0.8540	0.8540	0.8540	0.8540
	0.2	0.8350	0.8260	0.8240	0.8261	0.8261
	0.4	0.8107	0.7968	0.7932	0.7937	0.7937
	0.5	0.7956	0.7806	0.7764	0.7758	0.7758
	0.8	0.7325	0.7210	0.7171	0.7149	0.7149
	1.0	0.6685	0.6684	0.6684	0.6684	0.6684
1.0	0.0	0.9867	0.9867	0.9867	0.9867	0.9867
	0.2	0.9498	0.9593	0.9665	0.9837	0.9837
	0.4	0.9306	0.9442	0.9545	0.9802	0.9802
	0.5	0.9265	0.9404	0.9511	0.9781	0.9781
	0.8	0.9357	0.9446	0.9520	0.9706	0.9707
	1.0	0.9644	0.9644	0.9644	0.9644	0.9644

Table 5 confirms the accuracy of the pseudospectral method for the system of TFPDEs through evaluating the ℓ_∞ norm of the residual error varying values of γ in Example 3.4. The ℓ_∞ norm of the residuals for both u and v indicates high accuracy of the numerical method since the residuals are in the range of 10^{-12} and 10^{-14}, respectively. The CPU times show that the method is efficient, as all computations take less than a quarter of a second, even as the residuals increase with γ. The time remains relatively stable, which is a positive aspect of the method's computational performance. The slight variations in error norms do not significantly affect the overall accuracy, suggesting that the method is stable and reliable for a range of fractional orders.

Table 5
Maximum residual error for Example 3.4 for $M = 10$, $N = 20$, $q = 5$, and $h = 1$ with varying γ values.

	$\gamma = 0.1$	$\gamma = 0.3$	$\gamma = 0.5$	$\gamma = 0.7$	$\gamma = 0.9$
ℓ_∞ norm of $Res[u]$	1.3960×10^{-12}	2.1285×10^{-12}	3.6644×10^{-12}	1.2990×10^{-12}	6.6083×10^{-12}
ℓ_∞ norm of $Res[v]$	9.2149×10^{-14}	2.1183×10^{-13}	1.3323×10^{-13}	9.3481×10^{-14}	1.0059×10^{-13}
CPU time (s)	0.192118	0.197574	0.232721	0.207347	0.189793

Table 6
ℓ_2 and ℓ_∞ norms of the absolute error for Example 3.5 for various values of N_x, N_y, and M with $\gamma = 0.5$, $h = 1$, and $q = 5$.

(N_x, N_y, M)	(4, 4, 4)	(5, 5, 4)	(5, 5, 5)	(7, 7, 5)	(10, 10, 7)	(10, 10, 10)
ℓ_2 norm	1.9877×10^{-6}	2.0239×10^{-6}	9.9849×10^{-7}	1.0196×10^{-6}	3.5272×10^{-7}	1.1195×10^{-7}
ℓ_∞ norm	8.0239×10^{-6}	8.0174×10^{-6}	3.9634×10^{-6}	3.9809×10^{-6}	1.3736×10^{-6}	5.4198×10^{-7}
CPU time (s)	0.0484	0.0541	0.0610	0.3327	5.2471	7.6765

Table 7
ℓ_2 and ℓ_∞ norms of the absolute error for Example 3.5 for distinct values of γ with $N_x = N_y = 10$, $M = 4$, $h = 1$, and $q = 5$.

	$\gamma = 0.1$	$\gamma = 0.3$	$\gamma = 0.5$	$\gamma = 0.7$	$\gamma = 0.9$
ℓ_2 norm	2.1616×10^{-7}	9.4142×10^{-7}	2.0999×10^{-6}	3.4840×10^{-6}	3.1844×10^{-6}
ℓ_∞ norm	7.6752×10^{-7}	3.4188×10^{-6}	8.0590×10^{-6}	1.4512×10^{-5}	1.4280×10^{-5}
CPU time (s)	1.0027	1.0177	1.0165	0.9993	1.0461

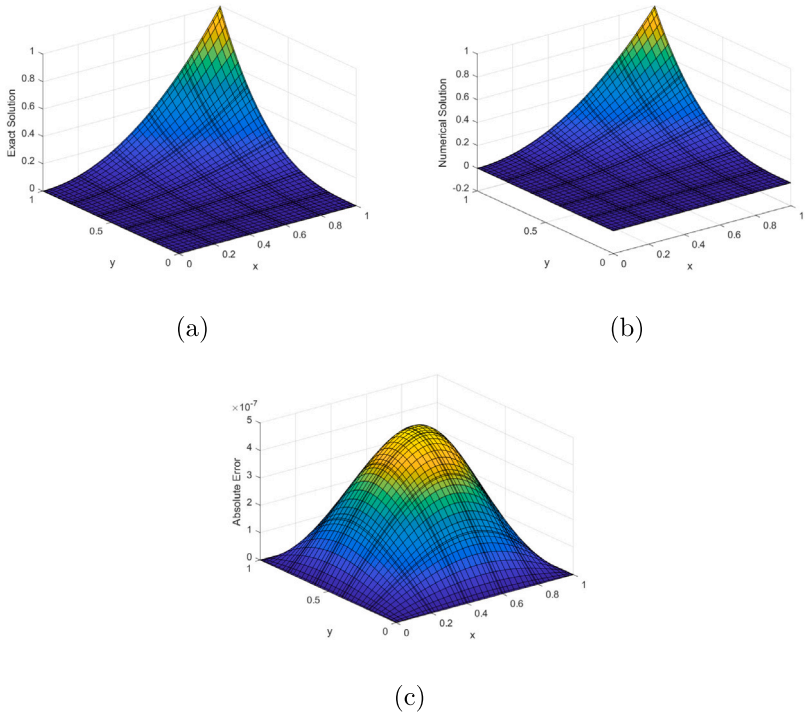

Fig. 4. Exact solution, numerical solutions and absolute error at $t = 1$ for Example 3.5 with $\gamma = 0.5$ and $N_x = N_y = M = 10$, $h = 1$ and $q = 5$.

Example 3.5. We examine a linear two-dimensional time-fractional diffusion equation in this example, presented by Oloniiju et al. [33]

$$ {}_0^C D_t^\gamma u + \frac{\partial^2 u}{\partial x^2} + \frac{\partial^2 u}{\partial y^2} = g(x, y, t), \qquad 0 < \gamma \leq 1, $$

with exact solution expressed as $u(x, y, t) = x^2 y^3 t^2$, and $g(x, y, t) = \frac{2}{\Gamma(3-\gamma)} x^2 y^3 t^{2-\gamma} + 2y^3 t^2 + 6x^2 y t^2$. The equation is solved subject to $u(x, y, 0) = 0$, $u(0, y, t) = u(x, 0, t) = 0$, $u(1, y, t) = y^3 t^2$ and $u(x, 1, t) = x^2 t^2$.

Tables 6 and 7 present the error norms for the absolute errors for Example 3.5. Table 6 investigates the effect of using different grid sizes in both spatial and temporal dimensions. The results demonstrate high accuracy for various combinations of grid point numbers. The accuracy of the results improves as the number of grid points increases. The displayed results illustrate the typical behavior of the method where finer grids lead to greater accuracy at the expense of longer computation times. The method's accuracy for different fractional orders γ is shown in Table 7. The small magnitude of error norms indicates highly accurate solutions. The method's efficiency is also emphasized by the minimal CPU time required to achieve these results. Fig. 5 shows the close agreement between the approximate and analytic solutions, which validates the accuracy of the pseudospectral method for TFPDEs (see Fig. 4).

4. Applications to thermal diffusion on a disk

The time-fractional thermal diffusion equation is an extension of the classical heat equation, incorporating a fractional derivative to model anomalous diffusion processes observed in various natural and industrial phenomena. Such models are particularly important for capturing

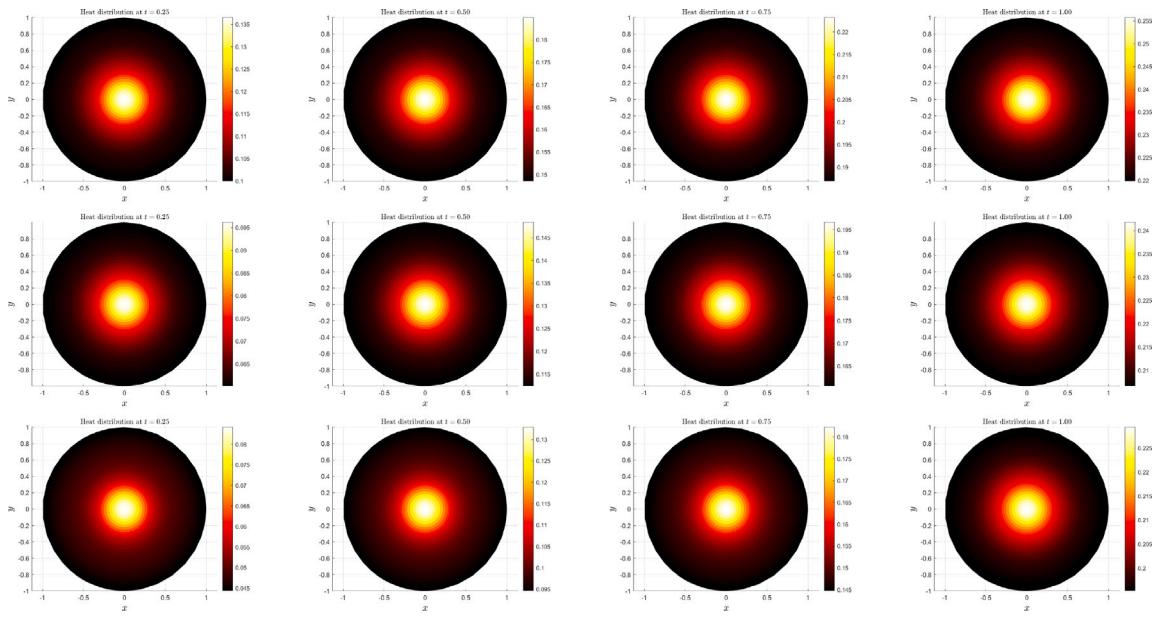

Fig. 5. Temperature distribution on the disk for the time-independent heat source centered at the origin with intensity $A = 10$, spread $\sigma_x = \sigma_y = 0.1$ and thermal diffusivity $\kappa = 5$ for different fractional orders, top: $\gamma = 0.55$, middle: $\gamma = 0.85$ and bottom: $\gamma = 1.0$.

non-local and history-dependent effects in materials where standard diffusion equations fail to accurately describe the behavior. This section explores the use of the pseudospectral method to approximate the solution of the time-fractional thermal diffusion equation, including a source term, within a two-dimensional disk. The choice of a disk geometry is motivated by its relevance in many practical applications, such as heat conduction in circular plates, semiconductor wafers, and other disk-shaped materials where thermal management is crucial. In cylindrical coordinates (r, θ), with $r \in [0, R]$ representing the radial distance and $\theta \in [0, 2\pi]$ the angular coordinate, the governing equation for thermal diffusion is given by:

$$ {}_0^C D_t^\gamma u = \kappa \left(\frac{1}{r} \frac{\partial}{\partial r} \left(r \frac{\partial u}{\partial r} \right) + \frac{1}{r^2} \frac{\partial^2 u}{\partial \theta^2} \right) + g(r, \theta, t), \quad 0 < \gamma \leq 1, \tag{44} $$

where $u(r, \theta, t)$ denotes the temperature distribution, ${}_0^C D_t^\gamma$ is the Caputo time-fractional derivative of order γ, κ is the thermal diffusivity coefficient, and $g(r, \theta, t)$ represents the source term accounting for internal heat generation or absorption. This formulation of the heat transfer process captures the diffusion of thermal energy within a disk, allowing for a more realistic representation of processes where non-Fickian diffusion occurs. The boundary and initial conditions are typically specified to ensure a well-posed problem. In this case, however, we consider a zero initial condition and a Neumann boundary condition on the boundaries of the disk. This section will detail the implementation of the pseudospectral method for this class of problems in capturing the thermal diffusion dynamics on a disk. To illustrate, we consider a localized heat source on the disk. The assumption is that the heat source is concentrated in a small region of the disk, such as a circular spot. Assume that the heat source is centered at (x_b, y_b) and has a certain intensity and spread, we can define a Gaussian source term

$$ g(r, \theta) = A \exp\left(-\frac{(x - x_b)^2}{2\sigma_x^2} \right) \exp\left(-\frac{(y - y_b)^2}{2\sigma_y^2} \right), \tag{45} $$

where $x = r\cos(\theta)$, $y = r\sin(\theta)$, A is the maximum heat intensity at the center of the heat source, σ_x and σ_y are the spread of the heat in the x- and y- directions, respectively, and by extension the radial and angular spread of the heat. Suppose we want to consider a source term which gradually comes on at $t > 0$ and is zero for $t \leq 0$, then a good candidate for the time-dependent source term will include the Heaviside step function, $H(t)$, which is equal to zero for $t \leq 0$ and smooth ramping function so that the time-dependent source term is now given an

$$ g(r, \theta, t) = A \exp\left(-\frac{(x - x_b)^2}{2\sigma_x^2} \right) \exp\left(-\frac{(y - y_b)^2}{2\sigma_y^2} \right) H(t)(1 - e^{-\nu t}), \tag{46} $$

where $(1 - e^{-\nu t})$ models a smooth increase in intensity, and ν controls the speed of the increase and the time-dependent ramp-up of the heat source.

The simulated results in Figs. 5 and 6 illustrate the thermal diffusion behavior on a disk for different fractional orders $\gamma = 0.55, 0.85, 1.0$, comparing both time-dependent and time-independent heat sources. These results illuminate how the anomalous diffusion process, governed by the fractional differential operator, influences the heat distribution on the disk over time. As time t progresses, the temperature distribution across the disk increases for both cases of the heat source, indicating that heat is diffusing into the domain. This is expected as more energy is introduced into the system over time, whether from a constant source or a time-varying one. The increase in temperature is uniform and smooth, characteristic of the diffusion process, but the rate of heat accumulation varies with the fractional order of the differential equation.

The comparison across different fractional orders reveals a critical observation: lower fractional orders ($\gamma = 0.55$) result in higher overall temperatures on the disk, while higher orders ($\gamma = 0.85, 1.0$) show progressively lower temperatures. This trend is consistent for both time-dependent and time-independent heat sources. The fractional derivative represents a form of "memory effect" in the diffusion process. The system exhibits subdiffusive behavior at $\gamma = 0.55$, meaning the heat diffuses more slowly than classical diffusion ($\gamma = 1$). This slower spread results in a more localized heat accumulation within the disk, leading to higher temperatures. For the classical case, $\gamma = 1.0$, the heat diffuses more efficiently on the disk, leading to a more uniform distribution and lower peak temperatures compared to lower fractional orders. As expected, $\gamma = 0.85$ shows intermediate behavior between the subdiffusive and classical diffusion cases. The time-dependent heat source results in a lower temperature distribution across the disk than the time-independent source. This difference can be attributed to the nature of the heat source. On the one hand, initially, at $t = 0$, the heat source is zero for the time-dependent heat source, meaning no heat is being added to the system. The source term increases as time

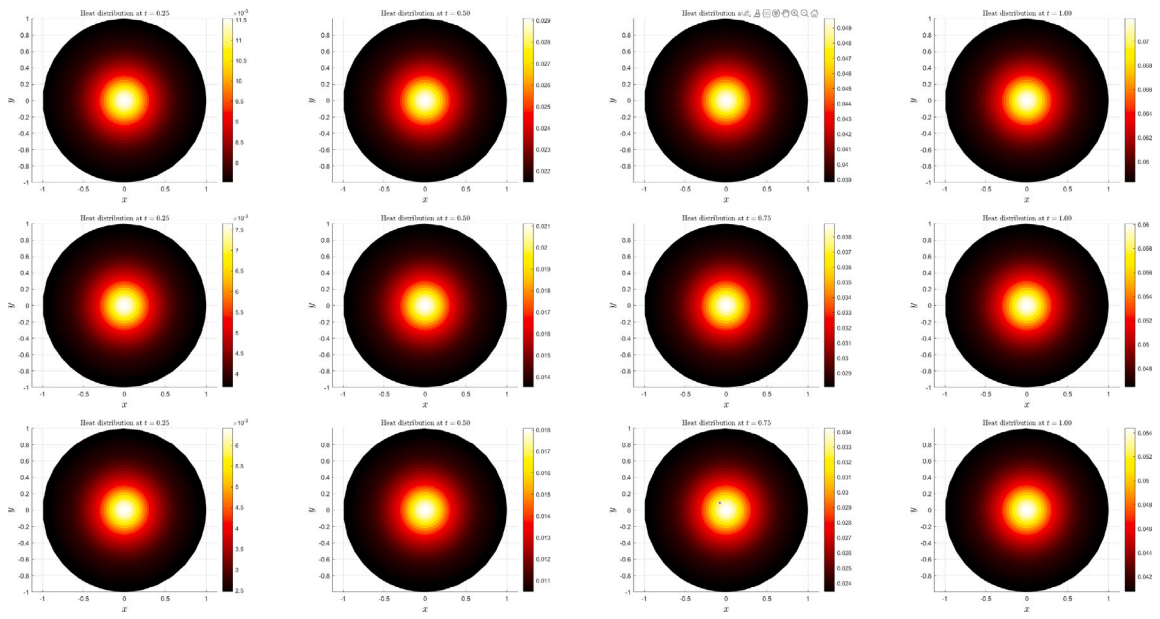

Fig. 6. Temperature distribution on the disk for the time-dependent heat source centered at the origin with intensity $A = 10$, spread $\sigma_x = \sigma_y = 0.1$, temporal ramp-up coefficient $\nu = 0.5$, and thermal diffusivity $\kappa = 5$ for different fractional orders, top: $\gamma = 0.55$, middle: $\gamma = 0.85$ and bottom: $\gamma = 1.0$.

progresses, gradually introducing heat into the system. This ramping-up process delays the heat accumulation on the disk, resulting in lower temperatures at any given time compared to the time-independent case. On the other hand, the source provides a constant supply of heat from the start for the time-independent heat source. As a result, heat begins to accumulate immediately, leading to higher initial and subsequent temperatures. This continuous and steady input allows the system to reach higher temperatures more quickly.

The results have significant practical implications in scenarios where thermal management is crucial. Higher temperatures can be expected due to localized heat accumulation for materials or systems with a subdiffusive nature ($\gamma < 1$). This might be beneficial in processes requiring high-temperature maintenance, such as certain manufacturing techniques, or it could present a risk in systems where overheating is a concern. Conversely, heat dissipates more effectively for materials with classical diffusion behavior ($\gamma = 1$), resulting in a more uniform and controlled temperature distribution. In applications with time-varying heat sources, delayed heat accumulation can be advantageous in preventing thermal shock, allowing gradual heating of the system. For steady-state heat sources, immediate heating is beneficial when a quick thermal response is required, but it could also increase the risk of overheating if not adequately managed. Overall, the analysis emphasizes the importance of understanding the diffusion characteristics of materials and the nature of heat sources in designing systems for optimal thermal performance and safety.

5. Concluding remarks

This study presents the development of a pseudospectral method for solving time-fractional PDEs. The technique used the Lagrange interpolating polynomials for approximating the solution in the spatial dimensions and the first-kind shifted Chebyshev polynomials in the temporal dimension. The spatial domain was divided into overlapping subdomains of equal length. The method was applied to both one-dimensional and two-dimensional TFPDEs, and the examples presented confirmed its accuracy, reliability, and efficiency. The small magnitude of the ℓ_2 and ℓ_∞ norms of the difference error, along with the residual errors, highlighted the approach's high accuracy, which likely derives from the non-local nature of the spectral method. It was also demonstrated that the numerical solutions closely match the exact solutions, with minimal oscillatory errors that do not significantly impact overall accuracy. The consistently low computational times indicate that the method is efficient and accurate in solving the resulting system of algebraic equations. Although the overlapping partitioned domain approach improves accuracy, it also introduces redundancy in the shared collocation points. However, the presence of overlap allows for natural patching of solutions at shared points, which improves the propagation of boundary information between adjacent subdomains. This overlap contributes to the stability of the numerical scheme. A lack of overlap may lead to numerical instability or reduced accuracy at the endpoints of the subdomains due to the absence of shared collocation or interpolation points. So, while a non-overlapping partitioned domains method is theoretically viable and very likely more computationally efficient, our choice of overlapping subdomains is a pragmatic trade-off. The consistent performance across various values of γ, combined with the minimal residual errors and stable CPU times, validated the robustness of the pseudospectral method. The numerical results confirmed that the numerical approach effectively captures the behavior of fractional differential equations, including the complex dynamics introduced by fractional orders. A comparison between the approximate and exact solutions showed strong agreement, further validating the method's accuracy and applicability.

This study also investigated heat transfer on a disk through the proposed pseudospectral method. The analysis of thermal diffusion behavior on a disk demonstrated how the fractional nature of the equation influences heat distribution and accumulation. The simulation results indicated that a lower fractional order, γ, resulted in a higher overall temperature, whereas a higher fractional order, γ, corresponds to a progressively lower temperature. This elevated temperature in a material exhibiting subdiffusive behavior ($\gamma < 1$) can be advantageous for processes that require sustained high temperature but may also pose overheating risks in sensitive systems. In contrast, the results also showed that materials that exhibit classical diffusion behavior ($\gamma = 1$) allow for more efficient heat dissipation, leading to a more controlled temperature distribution across the disk.

Overall, the study demonstrated that the pseudospectral method is a robust, efficient, and reliable approach for time-fractional PDEs, making it a valuable tool for both researchers and practitioners. The accuracy, driven by the method's spectral properties, and the computational efficiency make it highly suitable for a broad range of fractional calculus applications, such as scenarios requiring precise thermal management and analysis.

CRediT authorship contribution statement

Nancy Mukwevho: Writing – original draft, Methodology, Investigation. **Olumuyiwa Otegbeye:** Writing – review & editing, Visualization, Supervision, Methodology, Investigation. **Shina Daniel Oloniiju:** Writing – review & editing, Visualization, Validation, Supervision, Methodology, Investigation, Conceptualization.

Declaration of competing interest

The authors declare that they have no known competing financial interests or personal relationships that could have appeared to influence the work reported in this paper.

Acknowledgments

This work is based on the research supported in part by the National Research Foundation of South Africa (Ref Number: TTK2204163593).

Data availability

No data was used for the research described in the article.

References

[1] Alexander I. Fedorchenko, Introduction to Fractional Calculus, vol. 10.2.1, Czech Republic, 2008, pp. 1890–6887.
[2] HongGuang Sun, Yong Zhang, Dumitru Baleanu, Wen Chen, YangQuan Chen, A new collection of real-world applications of fractional calculus in science and engineering, Commun. Nonlinear Sci. Numer. Simul. 64 (2018) 213–231.
[3] J.A. Tenreiro Machado, Manuel F. Silva, Ramiro S. Barbosa, Isabel S. Jesus, Cecília M. Reis, Maria G. Marcos, Alexandra F. Galhano, Some applications of fractional calculus in engineering, Math. Probl. Eng. 2010 (1) (2010) 639801.
[4] H.M. Srivastava, Devendra Kumar, Jagdev Singh, An efficient analytical technique for fractional model of vibration equation, Appl. Math. Model. 45 (2017) 192–204.
[5] B.A. Jacobs, C. Harley, Application of nonlinear time-fractional partial differential equations to image processing via hybrid Laplace transform method, J. Math. Univ. Tokushima 2018 (1) (2018) 8924547.
[6] Saima Rashid, Khadija Tul Kubra, Asia Rauf, Yu-Ming Chu, YS Hamed, New numerical approach for time-fractional partial differential equations arising in physical system involving natural decomposition method, Phys. Scr. 96 (10) (2021) 105204.
[7] Jagdev Singh, Devendra Kumar, Adem Kılıçman, Numerical solutions of nonlinear fractional partial differential equations arising in spatial diffusion of biological populations, in: Abstract and Applied Analysis, Vol. 2014, Wiley Online Library, 2014, 535793.
[8] Vineet K. Srivastava, Sunil Kumar, Mukesh K. Awasthi, Brajesh Kumar Singh, Two-dimensional time fractional-order biological population model and its analytical solution, Egypt. J. Basic Appl. Sci. 1 (1) (2014) 71–76.
[9] Melike Kaplan, Ahmet Bekir, A novel analytical method for time-fractional differential equations, Optik 127 (20) (2016) 8209–8214.
[10] Aisha Abdullah Alderremy, Rasool Shah, Nehad Ali Shah, Shaban Aly, Kamsing Nonlaopon, Comparison of two modified analytical approaches for the systems of time fractional partial differential equations, AIMS Math. 8 (3) (2023) 7142–7162.
[11] Alemu Senbeta Bekela, Melisew Tefera Belachew, Getinet Alemayehu Wole, A numerical method using Laplace-like transform and variational theory for solving time-fractional nonlinear partial differential equations with proportional delay, Adv. Difference Equ. 2020 (1) (2020) 586.
[12] Rashid Nawaz, Rashid Ashraf, Laiq Zada, Hijaz Ahmad, Muhammad Farooq, Imtiaz Ahmad, Chutarat Tearnbucha, Weerawat Sudsutad, New approximate solutions to time fractional order partial differential equations optimal auxiliary function method, Therm. Sci. 27 (Spec. Issue 1) (2023) 9–17.
[13] Roberto Garrappa, Numerical solution of fractional differential equations: A survey and a software tutorial, Mathematics 6 (2) (2018) 16.
[14] Ji Lin, Lianpeng Shi, Sergiy Reutskiy, Jun Lu, Numerical treatment of multi-dimensional time-fractional Benjamin–bona–mahony–Burgers equations in arbitrary domains with a novel improvised RBF-based method, Comput. Math. Appl. 167 (2024) 178–198.
[15] Ji Lin, Jinge Bai, Sergiy Reutskiy, Jun Lu, A novel RBF-based meshless method for solving time-fractional transport equations in 2D and 3D arbitrary domains, Eng. Comput. 39 (3) (2023) 1905–1922.
[16] Hijaz Ahmad, Ali Akgül, Tufail A Khan, Predrag S Stanimirović, Yu-Ming Chu, New perspective on the conventional solutions of the nonlinear time-fractional partial differential equations, Complexity 2020 (1) (2020) 8829017.
[17] Mardo Herrera, Shweta Srivastava, César Torres, Analysis and numerical simulation of the time fractional diffusion equation by using mimetic finite differences, Authorea Prepr. (2022).
[18] Pradip Roul, V.M.K. Prasad Goura, Roberto Cavoretto, A numerical technique based on b-spline for a class of time-fractional diffusion equation, Numer. Methods Partial Differential Equations 39 (1) (2023) 45–64.
[19] Rania Saadeh, Ahmad Qazza, Aliaa Burqan, Shrideh Al-Omari, On time fractional partial differential equations and their solution by certain formable transform decomposition method, Comput. Model. Eng. Sci. 136 (3) (2023) 3121–3139.
[20] Umer Hayat, Abid Kamran, Bibi Ambreen, Ahmet Yildrim, Syed Tauseef Mohyud-Din, On system of time-fractional partial differential equations, Walailak J. Sci. Technol. (WJST) 10 (5) (2013) 437–448.
[21] Ali Shokri, Soheila Mirzaei, Numerical study of the two-term time-fractional differential equation using the Lagrange polynomial pseudo-spectral method, Alex. Eng. J. 59 (5) (2020) 3163–3169.
[22] Haifa Bin Jebreen, Carlo Cattani, Solving time-fractional partial differential equation using Chebyshev cardinal functions, Axioms 11 (11) (2022) 642.
[23] E.M. Abdelghany, W.M. Abd-Elhameed, G.M. Moatimid, et al., Petrov-Galerkin lucas polynomials approach for solving the time-fractional diffusion equation, Math. Syst. Sci. 3 (1) (2023) 3013, 2025.
[24] Ahmed Gamal Atta, Waleed Mohamed Abd-Elhameed, Youssri Hassan Youssri, Approximate collocation solution for the time-fractional Newell-Whitehead-Segel equation, J. Appl. Comput. Mech. 11 (2) (2025) 529–540.
[25] Ahmed Gamal Atta, Youssri Hassan Youssri, Enhanced spectral collocation Gegenbauer approach for the time-fractional Fisher equation, Math. Methods Appl. Sci. 47 (18) (2024) 14173–14187.
[26] Feng Chen, Qinwu Xu, Jan S. Hesthaven, A multi-domain spectral method for time-fractional differential equations, J. Comput. Phys. 293 (2015) 157–172.
[27] Hoda F. Ahmed, Waleed A. Hashem, A fully spectral tau method for a class of linear and nonlinear variable-order time-fractional partial differential equations in multi-dimensions, Math. Comput. Simulation 214 (2023) 388–408.
[28] Ahmed G Atta, Waleed M Abd-Elhameed, Galal M Moatimid, Youssri H Youssri, Novel spectral schemes to fractional problems with nonsmooth solutions, Math. Methods Appl. Sci. 46 (13) (2023) 14745–14764.
[29] Richard Ernest Bellman, Robert E. Kalaba, Quasilinearization and Nonlinear Boundary-Value Problems, RAND Corporation, Santa Monica, CA, 1965.
[30] L.N. Trefethen, Finite difference methods, J. Comput. Phys. 100 (1996) 123–145.
[31] Zaid Odibat, Shaher Momani, Numerical methods for nonlinear partial differential equations of fractional order, Appl. Math. Model. 32 (1) (2008) 28–39.
[32] Rasool Shah, Hassan Khan, Umar Farooq, Dumitru Baleanu, Poom Kumam, Muhammad Arif, A new analytical technique to solve system of fractional-order partial differential equations, IEEE Access 7 (2019) 150037–150050.
[33] S. Oloniiju, N. Nkomo, S. Goqo, Precious Sibanda, Shifted Chebyshev spectral method for two-dimensional space-time fractional partial differential equations, Preprints (2022) 2022050138.